A geodynamic framework for eastern Mediterranean kinematics

Paul Lundgren[1], Domenico Giardini[2], and Raymond M. Russo[3]

Abstract. We use a finite element model incorporating plate motion boundary conditions, fault constraints, and space geodetic velocities to calculate **eastern Mediterranean plate kinematics** and to estimate the motion of the region's major faults. We then use subsets of these constraints to generate models testing different scenarios of driving forces (slab roll-back at the Hellenic arc, Arabian plate push, gravitational collapse of W. Anatolia) to match the expected pattern of deformation. We find that models combining only trench rollback and Arabian push are unable to provide a good match to the observed deformation across western Anatolia and the Aegean and that we need to introduce the effects of mantle corner flow and gravitational collapse to fit observations.

plate tectonics
finite element modeling plate deformation
GPS geodynamics

Introduction

The tectonics of Anatolia and the Aegean have long been recognized as being an effect of the Alpine-Himalayan collision [*McKenzie,* 1972]. Geology, seismology and the advent of space geodesy have provided key constraints to test models of the large-scale regional tectonics and dynamics [*Wdowinski et al.,* 1989; *Oral et al.,* 1993; *Meijer and Wortel,* 1997].

A large uncertainty remains on the dynamics active in the Aegean, with contrasting models put forth to explain the kinematic observations and driving forces proposed for the regional tectonics. Much attention was paid to the westward extrusion of Anatolia towards a fixed Adriatic as the driving mechanism for Aegean dynamics [*Taymaz et al.,* 1991]; others favor the gravitational collapse of the continental lithosphere margin induced by the topographically generated potential energy gradient between central Greece and the deepest Hellenic arc [*Hatzfeld et al.,* 1997; *Davies et al.,* 1997]; or the rollback of the African plate subducting at the Hellenic arc as the main driving factor [*Oral et al.,* 1993; *LePichon et al.,* 1995; *Meijer and Wortel,* 1996, 1997; *Cianetti et al.,* 1997].

In this study we use finite element modeling to construct a model of regional kinematics constrained by space geodetic vectors and by the orientation and kinematic style of major faults. We then attempt to reproduce this model by imposing different sets of boundary conditions to gauge the relative contributions of trench suction and collisional models.

Finite element model

We solve for crustal displacements on an elastic spherical shell under plane stress conditions using a finite element approach which allows the mesh to be cut by faults [*Lundgren et *al.,* 1995] and imposing geodetic velocity vectors as prescribed nodal displacements. A Monte Carlo technique is used to estimate uncertainties in the model solutions based on the input uncertainties [*Peltzer and Saucier*, 1996]. In addition, we can input rigid truss bars connecting pairs of nodes in the model to impose prescribed relative displacement conditions. Since we solve an elastic problem, our model has no time dependence (kinematic versus dynamic), and imposed velocities enter into the model as displacements, with calculated solutions presented as velocities.

The model assumes a constant lithospheric thickness with the same material properties assigned to each element (Young's modulus $E = 7 \times 10^{10}$ Pa, and Poisson's ratio ν = 0.25). Boundary conditions are imposed as rigid plate motions with boundary rates calculated from the NUVEL-1A global plate model [*DeMets et al.*, 1994]. To simulate the crustal and lithospheric properties of different provinces in the Aegean and Anatolia, we apply different rigidity models (E). We use Global Positioning System (GPS) results for the Anatolia region from *Reilinger et al.* [1997] and Satellite Laser Ranging (SLR) results for the Aegean from *Noomen et al.* [1996]. In areas where data sets overlap there is close agreement between solutions, although SLR generally has greater uncertainties.

The finite element mesh we use encòmpasses the entire Mediterranean region from the Azores to Iran. This is done to extend the model into the relatively rigid interiors of the Eurasian, African, and Arabian plates. The boundary conditions are: W and N boundaries of Eurasia fixed, E boundary of Eurasia free; African and Arabian plates pushed at each boundary node's NUVEL-1A [*DeMets et al.*, 1994] velocity. Major faults extending between Eurasia and Africa/Arabia are left unconstrained. The Red Sea rift between Africa and Arabia is constrained to open with the NUVEL-1A velocity.

Model results and discussion

To test models of eastern Mediterranean tectonics we construct different numerical models for the plate margin kinematics. Our modeling approach hinges on three main assumptions:

1. The available geodetic data allow us to construct a regional-scale model that can be tested against the known seismotectonic elements and rates of the major fault structures and thus reproduces nature to the best of our geodesy constraints and finite-element modeling; this model is thus taken as the benchmark for all further modeling.
2. While the model is purely kinematic, we identify subsets of the geodetic constraints that we relate to specific tectonic forces allowing us to reproduce different dynamic scenarios, i.e. imposing the geodetic vectors along the Hellenic arc to simulate the effect of trench suction or using truss bars along the Western Anatolia margin to mimic gravitational lithospheric collapse [*Sonder and England*, 1989];
3. A 1-D evaluation of strain and strain-rate along an E-W minor arc cutting our model allows us to quantify the deformation pattern and highlight the different regions and patterns contributing to the regional geodynamics.

Our starting model (Fig. 1) is constructed by imposing far-field boundary conditions, all available space geodetic vectors (GPS/SLR), and the orientation and sense of faulting of the major faults for the Aegean and Anatolian regions. The displacement vectors at the grid points describe a deformation pattern that exactly reproduces the geodetic constraints and fits our current understanding of the regional tectonics. Indeed, in agreement with current models of seismic strain rates [e.g., *McKenzie*, 1972; *Kiratzi and Papazachos*, 1995; *Baker et al.*, 1997], we obtain 19-24 mm/yr rates on the North Anatolian Fault, lower rates across faults in the Aegean with normal motion across the Gulf of Corinth peaking at 6-12 mm/yr in agreement with observations of marine terraces [*Armijo et al.*, 1996], rates of less than 10 mm/yr in western Turkey, convergence at the Hellenic thrust of 33-36 mm/yr, and 10 mm/yr left-lateral slip along the East Anatolian Fault. The overall pattern demonstrates that the geodetic constraints are sufficient to calibrate a consistent regional model.

Our goal is to reproduce different geodynamic scenarios and broad patterns of strain rather than to highlight how deformation concentrates on individual faults. We thus use a simplified model F1 without faults in the Aegean and western Anatolia, with a zone of weak crust in the NW Aegean to decouple our tests from complications in the Dinarides and Balkans.

To compare the deformation patterns for different models, we display the strain and continuum rate tangential to a small circle about the Euler pole calculated for Anatolia (based on the GPS vectors, *Reilinger et al.*, [1997]). In Fig. 2 we show the strain and continuum rate parallel the arc shown in Fig. 1B (located 10° from the Euler pole). The profiles F1 confirm known tectonics but also reveals surprising characteristics:

- The bulk of Anatolia is mostly rigid; a small extensional component could be present, not exceeding an overall extension of 2 mm/yr across central and eastern Anatolia, a value close to the numerical precision of the GPS dataset, in agreement with earlier observations [*Reilinger et al.*, 1997].
- A pronounced extension, with corresponding increase in continuum motion moving toward the Aegean, takes place across western Anatolia; a N-S extension dominates the seismicity and neotectonic observations and has been related by several authors to the collapse of the continental lithosphere margin. Due to the chosen geometry, here we display only the ENE-WSW component of extension.
- The Aegean basin is under slight compression tangent the small circle, as confirmed by a recent, more complete compilation of GPS vectors across the whole area [*Reilinger et al.*, 1998]. The calculated strain pattern is in agreement with the proposed recent change of stress field in the Aegean from a NE-SW extensional regime to a NNW-SSE extensional regime [*Meijer and Wortel*, 1996] and points to an almost rigid Aegean plate, moving away from Anatolia on a more southerly trajectory.

We now seek to understand what subset of boundary conditions match the fully constrained crustal motions (Fig. 1). We present four models which test various combinations of plate forces. We have also examined the effects of varying the continuum material properties, with the expected result that the more heterogeneous models (shown here) attain more pronounced deformation in areas of relatively lower strength.

In the first model (Fig. 2, 3A) we only impose the NUVEL-1A constraints on the African and Arabian plates and GPS vectors on the northern Arabian plate margin and continental Anatolia. This allows us to match the motion of Anatolia as required (e.g. Fig. 1), but in the Aegean continuum rates diminish, resulting in compressional strain due to the dissipation of the push from Anatolia.

To test the effect of slab rollback or trench suction at the Hellenic Arc, the second model (Fig. 2, 3B) reverses the geodetic constraints, imposing SLR rates in the Aegean and turning off all other geodetic constraints and the plate boundary conditions of Arabia and Africa rotation. This model produces extensional strain across the Aegean, due to the dissipation of the trench retreat, but fails to pull Anatolia rigidly along at the observed rate and rotation, leaving eastern Anatolia with little motion. Even in models with uniform high rigidity and coupling of the Aegean-Anatolian province this model could not produce the correct pattern of velocities across Anatolia.

The third model (Fig. 2, 3C) simulates the combined effect of slab pull and plate push, and includes the SLR vectors at the Hellenic Arc, the NUVEL-1A far-field plate motions and GPS vectors south of the East Anatolian fault. This model comes closest to matching the fully constrained velocity pattern (Fig. 1), with the rotation of Anatolia similar to the GPS observations, and N-S extension in Greece, similar to observed earthquake focal mechanisms [e.g., *McKenzie*, 1972; *Kiratzi and Papazachos*, 1995; *Baker et al.*, 1997]. However, this model produces NE-SW extension in the central - southern Aegean in contrast to the current geologically or seismologically observed strain pattern [*Meijer and Wortel*, 1996; *Taymaz et al.*, 1991] and fails to concentrate the extensional strain in the Western Anatolia margin (profile F1 in Fig. 2A); as a result, the velocity profile in Fig. 2B is significantly lower than expected (confirming the results from *Cianetti et al.* [1996]).

The strain and velocity profiles (Fig. 2) highlight the effects of trench suction and plate push. Plate push at the eastern Anatolia margin will always result in compressional strains; by making the Anatolia plate more rigid, conforming to its expected rheology, Anatolia behaves as a true plate, transmitting the compression to its western margin. Pulling at the arc always results in extensional pattern in the Aegean, with intensity and the rate fall-off distance inversely proportional to rigidity. The question remains: how to achieve the observed strain and velocity profiles from a model with reasonable material properties and the commonly accepted tectonic forces?

We find two mechanisms capable of concentrating the deformation in the western Anatolia margin, achieving a good match to the F1 profiles in Fig. 2. Firstly, we simulate the conditions where the weakest part of the model is indeed the Anatolia margin, as a result of pervasive extension sharply reducing the shear strength of its brittle layer. We modify model C by increasing the strength of the Aegean crust an order of magnitude; conversely, the Aegean behaves almost rigidly, transferring the trench suction to the only area now capable of significant deformation, the western Anatolia margin, and the strain and rate profiles (C' in Fig. 2) achieve a better match to profiles F1. A high rigidity Aegean plate has been proposed by *Sonder and England* [1989]. A rigid Aegea can alternatively be viewed as a proxy for basal tractions due to mantle corner flow as suggested by *Wdowinski et al.*, [1989].

A second possibility is to invoke a distinctly different physical mechanism, i.e. the gravitational collapse of the unsustained continental lithospheric margin, to explain the increase in velocities from central Anatolia to western Anatolia.

This mechanism is central to modern interpretations of subduction initiation and marginal basin formation in the Mediterranean and continental highland deformation (*Faccenna et al.*, 1996; *Jones et al.*, 1996; *England and Molnar*, 1997). We obtain model D (Fig. 3D) by adding rigid truss bars to model C to impose the extension derived from the GPS vectors (Fig. 1A) across western Anatolia (truss bars only impose relative, not absolute constraints) leaving Anatolia and the Aegean free to partition the remaining strains according to the adopted rigidities. Model D obtains results very similar to profiles C', but features the nominal rigidity for the Aegean and Anatolia and a lower rigidity (1/10 nominal) for western Anatolia. This suggests that gravitational extension across western Anatolia can reproduce much of the observed strain and motion along the arc tangential to the rotation of Anatolia.

Conclusions

We employ a 2-D elastic shell finite element technique to test models of Anatolian-Aegean geodynamics. The model that is constrained by the available space geodetic data gives fault rates across major faults that agree with independent estimates for the Gulf of Corinth, and provide estimates for other major faults where greater geologic uncertainty exists. We find that the modeled kinematics of the region require both fast trenchward motion of the Hellenic arc and extrusion of Anatolia due to the collision of Arabia. Additional driving mechanisms are required to sustain the near constant high velocity observed across the Aegean and the sharp extension seen along the W. Anatolia margin, interpreted as the effect of gravitational lithospheric collapse.

Acknowledgments: We thank N. D'Agostino, C. Faccenna, M. Mattei for their stimulating discussion and the critical reviews of P. Meijer and an anonymous reviewer. Part of this work was done at the Jet Propulsion Laboratory, California Institute of Technology, under contract with the National Aeronautics and Space Administration.

REFERENCES

Armijo, R., B. Meyer, G. C. P. King, A. Rigo, and D. Papanastassiou, Quaternary evolution of the Corinth Rift and its implications for the Late Cenozoic evolution of the Aegean, *Geophys. J. Int.*, *126*, 11-53, 1996.

Baker, C., D. Hatzfeld, H. Lyon-Caen, E. Papadimitriou, and A. Rigo, Earthquake mechanisms of the Adriatic Sea and Western Greece: Implications for the oceanic subduction-continental collision transition, *Geophys. J. Int.*, *131*, 559-594, 1997.

Cianetti, S., P. Gasperini, M. Boccaletti, and C. Giunchi, Reproducing the velocity and stress fields in the Aegean region, *Geophys. Res. Lett.*, *24*, 2087-2090, 1997.

Davies, R., P. England, B. Parsons, H. Billiris, D. Paradissis, and G. Veis, Geodetic strain of Greece in the interval 1892-1992, *J. Geophys. Res.*, *102*, 24,571-24,588, 1997.

DeMets, C., R. G. Gordon, D. F. Argus, and S. Stein, Effect of recent revisions to the geomagnetic reversal time scale on estimates of current plate motions, *Geophys. Res. Lett.*, *21*, 2191-2194, 1994.

England, P., and P. Molnar, Active deformation of Asia: From kinematics to dynamics, *Science*, *278*, 647-650, 1997.

Faccenna, C., P. Davy, J. P. Brun, R. Funicello, D. Giardini, M. Mattei, and T. Nalpas, The dynamics of back-arc extension: An experimental approach to the opening of the Tyrrhenian Sea, *Geophys. J. Int.*, *126*, 781-795, 1996.

Hatzfeld, D., J. Martinod, G. Bastet, and P. Gautier, An analog experiment for the Aegean to describe the contribution of gravitational potential energy, *J. Geophys. Res.*, *102*, 649-659, 1997.

Jones, C. H., J. R. Unruh, and L. J. Sonder, The role of gravitational potential energy in active deformation in the southwestern United States, *Nature*, *381*, 37-41, 1996.

Kiratzi, A. A., and C. B. Papazachos, Active crustal deformation from the Azores triple junction to the Middle East, *Tectonophysics*, *243*, 1-24, 1995.

Le Pichon, X., N. Chamot-Rooke, and S. Lallemant, Geodetic determination of the kinematics of central Greece with respect to Europe: Implications for eastern Mediterranean tectonics, *J. Geophys. Res.*, *100*, 12,675-12,690, 1995.

Lundgren, P., F. Saucier, R. Palmer, and M. Langon, Alaska crustal deformation: Finite element modeling constrained by geologic and VLBI data, *J. Geophys. Res.*, *100*, 22,033-22,045, 1995.

McKenzie, D. P., Active tectonics of the Mediterranean region, *Geophys. J. R. Astron. Soc.*, *30*, 109-185, 1972.

Meijer, P. Th., and M. J. R. Wortel, Temporal variation in the stress field of the Aegean region, *Geophys. Res. Lett.*, *23*, 439-442, 1996.

Meijer, P. Th., and M. J. R. Wortel, Present-day dynamics of the Aegean region: A model analysis of the horizontal pattern of stress and deformation, *Tectonics*, *16*, 879-895, 1997.

Noomen, R., T. A. Springer, B. A. C. Ambrosius, K Herzberger, D. C. Kuijper, G. J. Mets, B. Overgaauw, and K. F. Wakker, Crustal deformations in the Mediterranean area computed from SLR and GPS observations, *J. Geodyn.*, *21*, 73-96, 1996.

Oral, M. B., R. E. Reilinger, M. N. Toksoz, A. A. Barka, and I. Kinik, Preliminary results of 1988 and 1990 GPS measurements in western Turkey and their tectonic implications, in *Contributions of Space Geodesy to Geodynamics: Crustal Dynamics, Geodyn. Ser.*, vol. 23, edited by D. E. Smith and D. L. Turcotte, pp. 139-176, AGU, Washington, D.C., 1993.

Peltzer, G. and F. Saucier, Present-day kinematics of Asia derived from geologic fault rates, *J. Geophys. Res.*, *101*, 27,943-27,956, 1996.

Reilinger, R. E., S. C. McClusky, M. B. Oral, R. W. King, M. N. Toksoz, A. A. Barka, I. Kinik, O. Lenk, and I. Sanli, Global Positioning System measurements of present-day crustal movements in the Arabia-Africa-Eurasia plate collision zone, *J. Geophys. Res.*, *102*, 9983-9999, 1997.

Reilinger, R. S. McClusky, R. King, N. Toksoz, A. Barka, C. Demir, G. Veis, A. Ouzounis, M. Prilepin, V. Kotzev, I. Georgiev, H. Kahle, H. Seeger, and A. Tealab, Velocity field for the eastern Mediterranean, Proceedings XXIII General Assembly, European Geophys. Soc., 1998.

Sonder, L. J., and P. C. England, Effects of a temperature dependent rheology on large-scale continental extension, *J. Geophys. Res.*, *94*, 7603-7619, 1989.

Taymaz, T., J. Jackson, and D. McKenzie, Active tectonics of the north and central Aegean Sea, *Geophys. J. Int.*, *106*, 433-490, 1991.

Wdowinski, S., R. J. O'Connell, and P. England, A continuum model of continental deformation above subduction zones: Application to the Andes and the Aegean, *J. Geophys. Res.*, *94*, 10,331-10,346, 1989.

P. Lundgren, Jet Propulsion Laboratory, California Institute of Technology, 4800 Oak Grove Dr., Pasadena, CA 91109. (e-mail: paul@dagobah.jpl.nasa.gov)

D. Giardini, Institute of Geophysics, ETH Honggerberg, CH-8093, Zurich, Switzerland. (e-mail: giardini@seismo.ifg.ethz.ch)

R. Russo, Department of Geological Sciences, Northwestern University, Evanston, Illinois, 60208. (e-mail: ray@earth.nwu.edu)

(Received May 18, 1998; revised July 23, 1998;
accepted September 17, 1998.)

[1]Jet Propulsion Lab., California Institute of Technology, Pasadena.

[2]Institute of Geophysics, ETH, Zurich, CH-8093 Switzerland.

[3]Dept. of Geological Sci., Northwestern University, Evanston, Illinois

Fig. 1. Fully constrained model. Eastern Mediterranean around the Aegean and Anatolia are shown. (A) GPS/SLR velocity vectors used to constrain model, with the areas of higher or lower rigidity shaded. (B) Continuum and fault motion solutions for this model. Gray arc defines small circle about the

Anatolia Euler pole of *Reilinger et al.* [1997]. The two black bars across this arc mark the 30 and 60° locations.

Fig. 2. Strain rate and motion tangential to the arc shown in Fig. 1B. Profiles go from the Hellenic trench (left) to the East Anatolian Fault (right). The labels adjacent each curve correspond to the corresponding subplot in Fig. 3, with the exception of F1 which corresponds to the solution in Fig. 1B, and curve C' which corresponds to a variation on the model in Fig. 3C with a strong Aegean (see text). (*Top*) Strain rate, positive values denote extension parallel the arc, negative values compression. (*Bottom*) Continuum displacement rate.

Fig. 3. Four models showing the effects of different geodynamic forcing. (A) Model forced by far-field boundary conditions and GPS motions in Central and SE Turkey. (B) Model forced only by SLR vectors in the Hellenic arc with no far-field plate forcing. (C) Model forced from Arabia and pulled by the Hellenic arc. (D) Same as in (C) but with extensional truss bars across western Anatolia (shown by the gray bars with their imposed rates labeled). The elastic model used in this case has nominal values for the Aegean and Anatolian crust ($E = 7\times10^{10}$ Pa) with a weaker W. Anatolian crust (1/10 nominal).

LUNDGREN ET AL.: EASTERN MEDITERRANEAN GEODYNAMICS

LUNDGREN ET AL.: EASTERN MEDITERRANEAN GEODYNAMICS

LUNDGREN ET AL.: EASTERN MEDITERRANEAN GEODYNAMICS

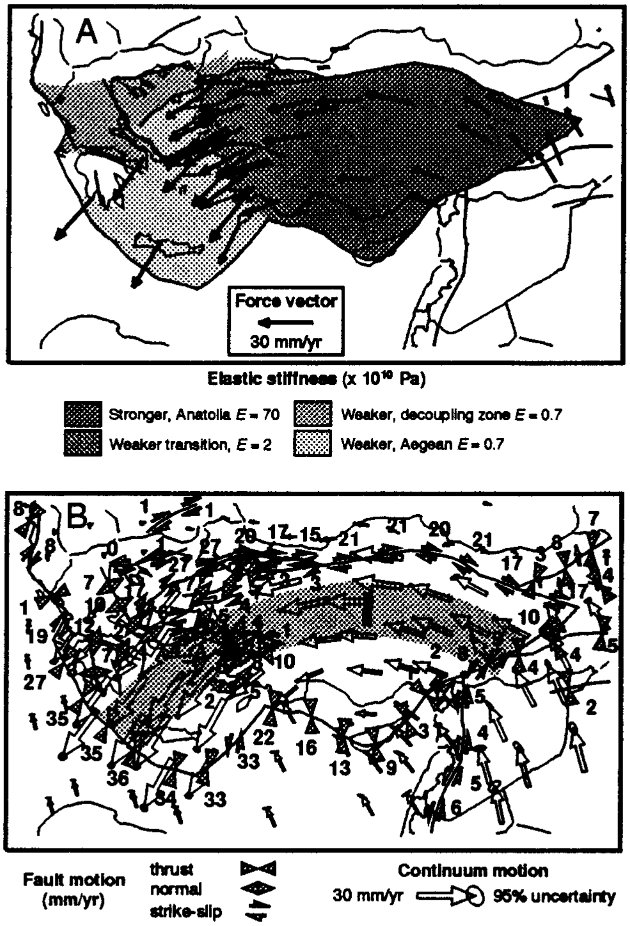
A
Force vector
30 mm/yr
Elastic stiffness (x 10^10 Pa)
Stronger, Anatolia E = 70
Weaker transition, E = 2
Weaker, decoupling zone E = 0.7
Weaker, Aegean E = 0.7
B
Fault motion
(mm/yr)
thrust
normal
strike-slip
Continuum motion
30 mm/yr
95% uncertainty

Figure 1

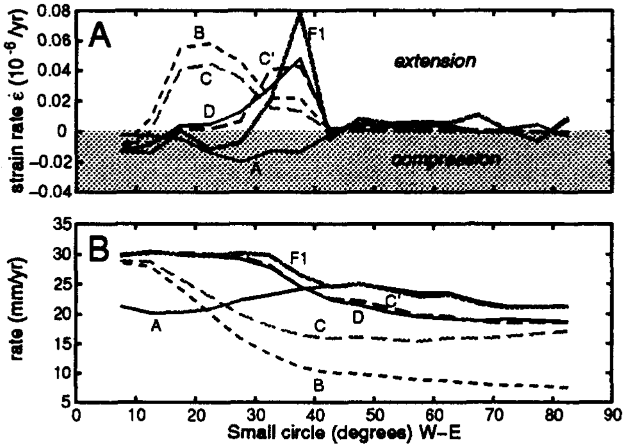
A
B
C
C'
D
F1
extension
compression
strain rate ε̇ (10⁻⁶/yr)
0.08
0.06
0.04
0.02
0
−0.02
−0.04
B
A
B
C
C'
D
F1
rate (mm/yr)
35
30
25
20
15
10
5
0
10
20
30
40
50
60
70
80
90
Small circle (degrees) W–E

Figure 2

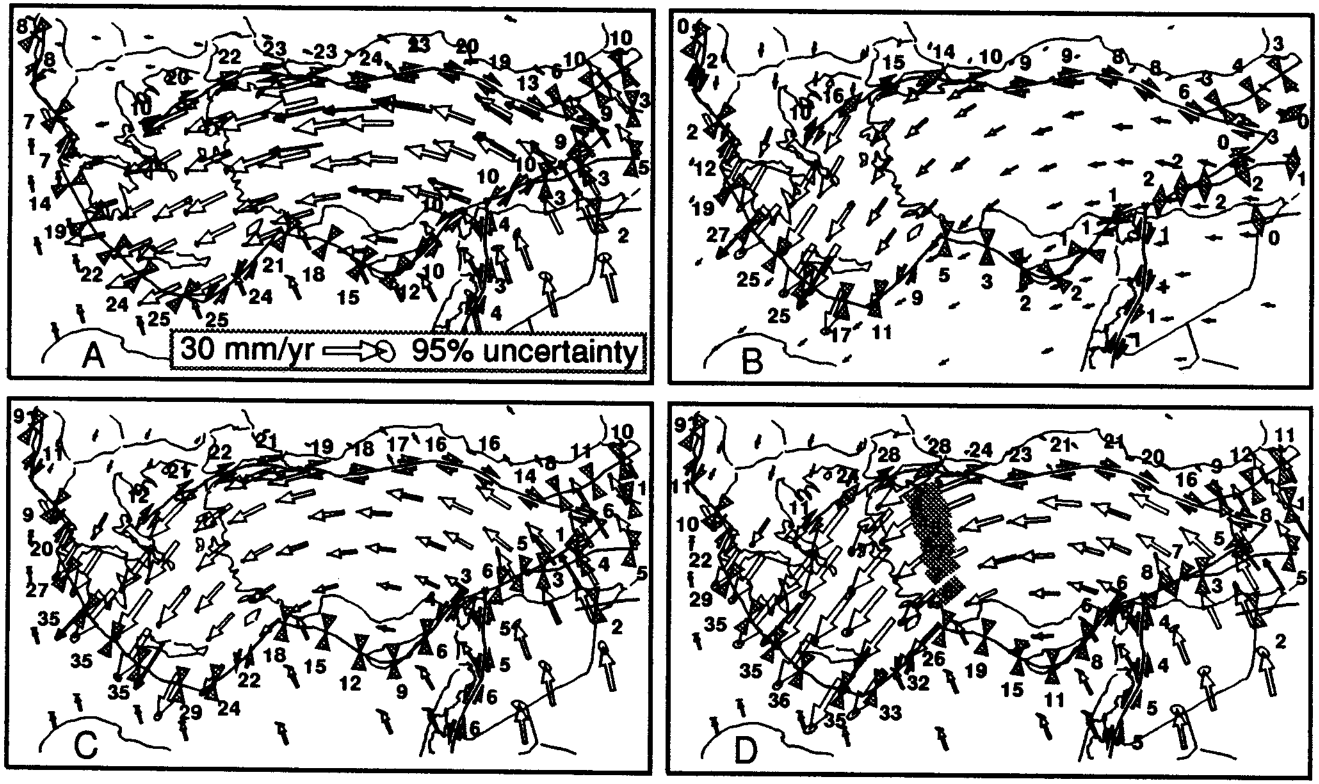

Figure 3

Lundgren, Giardini, and Russo, 1998